

Simulation and Experiments on a Valveless Micropump With Fluidic Diodes Based on Topology Optimization

Peng Zhou, Tianyi Zhang, Terrence W. Simon^{ID}, and Tianhong Cui^{ID}, *Senior Member, IEEE*

Abstract—Micropumps are microelectromechanical system (MEMS) devices that pump small quantities of liquids. They are used in many applications such as electronics cooling and drug delivery. Valveless fluid diode micropumps with no moving parts have recently attracted great interest in the MEMS community. In this paper, topology optimization is used to design two-dimensional, fixed-geometry, fluidic diodes of high diodicity, which is the ratio of pressure drops of forward to reverse flows. One of the fluidic diodes, of the Tesla type, shows a diodicity of over five. Another is of the nozzle-diffuser type. Both are experimentally and computationally demonstrated herein. Then the numerical simulation was applied to simplify the structures, and the two-dimensional geometry was converted into three-dimensional model for micropumps. Three-dimensional and unsteady numerical analyses of micropump fluid flow with optimized diodes were conducted for pumps of each of the two diode designs. The micropump with the Tesla-type fluidic diode reached a measured flow rate of 34 ml/h, consistent with the computed results and 2.2 times that of the nozzle-diffuser type micropump. The performance results show a high dependence on internal channel geometry. The two types show highest flow rates with an internal channel thickness of 200 μm . Demonstrated good repeatability and precise flow control show positive prospects for application. [2021-0144]

Index Terms—Fluidic diode, topology optimization, valveless pump.

I. INTRODUCTION

MICROPUMPS are microelectromechanical systems (MEMS) devices that pump small quantities (nanoliters or microliters) of fluid. They have been widely used in thermal control of electronics, measurement of volumes in the micro-scale, mixing of microfluidic streams, and medical applications [1]. For example, the piezoelectric actuation based valveless micropump has proved to be useful for drug delivery [2], and its application as an actuator for dynamic

cultures on ‘organs on a chip’ has gained recent attention [3]. Passive fluid diodes with no mechanical moving parts are used in valveless micropumps. They have attracted great interest due to their simple structures, compact sizes, lack of electromagnetic interferences, and easy integration [4]. The working mechanism of the valveless micropump is based on the difference of flow resistance between forward flow and back flow through internal channels [5].

Two commonly used valveless micropumps are based on either nozzle-diffuser channels or Tesla-type diodes. The nozzle-diffuser valveless micropump uses V-shaped channels that behave like nozzles when the flow is in one direction and like diffusers when the flow is in the opposite direction [4], [6], [7]. Chandrasekaran and Packirisamy studied the flow behavior of a nozzle-diffuser type valveless micropump with geometrical tuning using finite element modeling [8]. They proposed a method to design the best diffuser geometries using different diffuser angles. Then Yang and his group considered increasing the micropump flow rate by adding two-fin, or obstacle, structures into the nozzle-diffuser design [9]. However, the increased flow resistance offset the potential improvement. The Tesla-type valveless micropump gained interest after 1999 because of its high diodicity. Researchers [10] considered different structures of the Tesla valve flow-directing element. The diodes are complex channels (to be introduced below) that offer different flow losses for the two flow directions. Derakhshan *et al.* simulated flow behavior of the Tesla-type valveless micropump and optimized the dimensions of the diode to achieve higher diodicity and flow rate [11]. Kolahdouz suggested that the two-stage Tesla valve is the optimized design for a piezoelectric-driven micropump [12]. Most of the published work is focused on dimension or shape optimization of existing flow-directing elements [13]. Since the fundamental structures are not changed, performance improvement was limited.

Topology optimization is a systematic approach to optimize the layout of valve internal elements using a computational procedure for a given set of boundary conditions and constraints [14]. It has been successfully used to solve fluid-based problems, especially in the design of fluidic diodes with high diodicity [15]. Lin *et al.* used this method to optimize the Tesla-type valve and obtained fluidic diodes with diodicities of up to 8.87 [16]. Sato and his group proposed a bi-objective topology optimization method and designed a fluidic diode with lower pressure drop for the forward flow and higher pressure drop for the backward flow [17]. The published fluidic diodes were mainly used as fluidic resistance valves [18], and their application to valveless pumps was barely discussed.

Manuscript received July 9, 2021; revised October 25, 2021; accepted November 20, 2021. Date of publication December 28, 2021; date of current version April 4, 2022. This work was supported in part by the Minnesota Environment and Natural Resources Trust Fund as recommended by the Legislative-Citizen Commission on Minnesota Resources (LCCMR) and in part by the Minnesota Nano Center by the National Science Foundation through the National Nano Coordinated Infrastructure Network (NNCI) under Award ECCS-1542202. An earlier version of this paper was presented at the IEEE 34th International Conference on Micro Electro Mechanical Systems, in January 2021 [DOI: 10.1109/MEMMS51782.2021.9375273]. Subject Editor H. Jiang. (Corresponding author: Tianhong Cui.)

The authors are with the Department of Mechanical Engineering, University of Minnesota, Minneapolis, MN 55455 USA (e-mail: zhou1161@umn.edu; zhan6202@umn.edu; simon002@umn.edu; cuihx006@umn.edu).

This article has supplementary material provided by the authors and color versions of one or more figures available at <https://doi.org/10.1109/JMEMS.2021.3133469>.

Digital Object Identifier 10.1109/JMEMS.2021.3133469

Moreover, the scales of these published fluidic diodes were large relative to MEMS devices, further preventing application to MEMS-based micropumps [18].

This work seeks to investigate a microscale fluidic diode of high diodicity that can be used in valveless micropumps to achieve higher mass flow rate by using topology optimization and computational fluid dynamic (CFD) methods. MEMS technology is used to fabricate the fluidic diode-based valveless micropumps.

II. EXPERIMENTS AND ANALYSIS

A. Topology Optimization

The two-dimensional fluidic diode was first obtained using topology optimization based on the Density Model with Darcy interpolation. In short, the Navier-Stokes equations for forward and backward flows were solved. The ratio of pressure drop between the inlet and outlet for backward flow and forward flow was calculated as diodicity. To achieve high diodicity, the ratio of energy dissipation between backward and forward flow was set as the objective function for topological optimization [19]. A relatively low Reynold number of 100 was used for the calculation. The scale of a fluidic diode is primarily defined by the width of the inlet chamber. The different widths of the outlet and sizes of the computational domains were used to obtain fluidic diodes of different geometries. The diodicity of each fluidic diode was calculated to evaluate its performance.

The designed fluidic diodes with the highest diodicity were selected to employ in a valveless pump. The structure of the selected fluidic diode of the Tesla-type design was first simplified to remove extremely small features that cause excessive aspect ratios of the features that can challenge the fabrication process. The removed small structures are unnecessary and have little effect on performance. The performance characteristics of three-dimensional fluidic diodes of both types and of various thicknesses were also evaluated to optimize the thickness of valveless micropump.

Finally, CFD simulations of valveless micropumps with the selected fluidic diodes were applied. The nozzle-diffuser type valveless micropump of the same actuator size was simulated for comparison.

Commercial software COMSOL Multiphysics was used to solve the topology optimization for 2D structures, and CFD simulation was conducted for 2D and 3D structures by ANSYS Fluent.

B. Fabrication and Evaluation

MEMS technology was used to fabricate the valveless micropump with the topologically optimized Tesla-type fluidic diodes and with the conventional nozzle-diffuser diode to fabricate valveless micropumps for comparison. In order to capitalize upon repeated use of molds and low-cost processing technology, micropumps with a sandwich structure of two polymer films and an intermediate structural layer were designed and fabricated [20].

The fabrication process is shown in Fig. 1a. Lithography with negative photoresist SU8-100 was first performed on a silicon wafer. The thickness of the photoresist ranged from 150 μm to 250 μm , depending on the rotational speed of

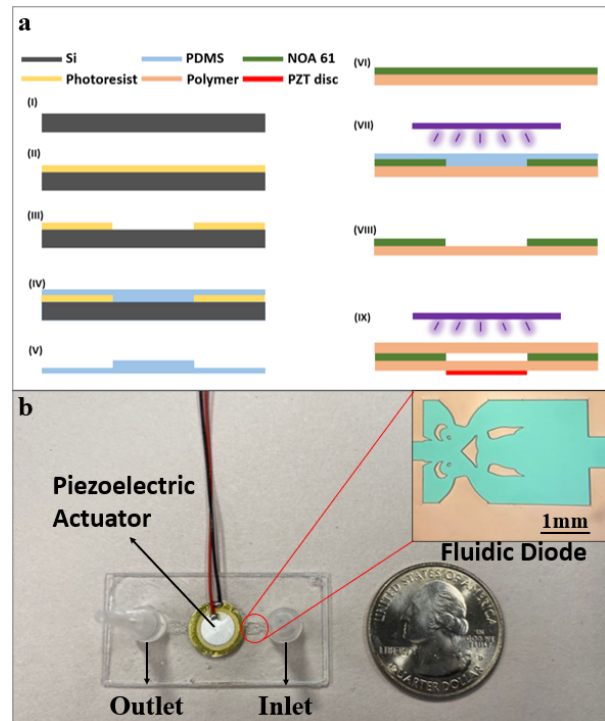


Fig. 1. (a) Schematic diagram of the fabrication process; (b) picture of the valveless micropump with the designed Tesla-type fluidic diode and a microscope image of the detailed structure.

the spin coating process. Polydimethylsiloxane (PDMS) was then poured on a silicon-based mold and cured to obtain a soft mold with mating structures. Then UV-curing glue, NOA61, was applied on the PDMS mold and covered with a UV-transparent polymer film. The NOA61 was partially cured under UV illumination, followed by replacement of the PDMS mold with another polymer sheet. More UV illumination was then applied to fully cure the NOA61. Finally, a piezoelectric (PZT) disc was attached to a polymer film to serve as the actuator. Fig. 1b shows details of the critical structures of the fabricated fluidic diode based valveless micropump based on the Tesla diode.

Characterization mainly includes measuring the amplitude of the PZT actuator (Fig. 1b), the flow rate of the micropump, and the pressure difference under operation. A function generator and a linear piezoelectric amplifier were used as the excitation source of the PZT actuator. A voltage of up to 100 V was applied to the PZT disc. The amplitude of the PZT actuator movement was measured by a laser vibrometer. The inlet and outlet of the micropump were connected to tubes of known diameters. The mass flow rate was calculated by placing the inlet and outlet tubes horizontally at the same level and measuring the displacement of the liquid meniscus in the tube within a specific period. In the pressure difference test, the inlet and outlet tubes were placed vertically and the pressure difference was determined by measuring the liquid level difference.

III. RESULTS AND DISCUSSION

Figures 2a and 2b show the computational domain before and after topology optimization. The size of the inlet and outlet, and the length and width of the rectangular computational domain were optimized for high diodicity.

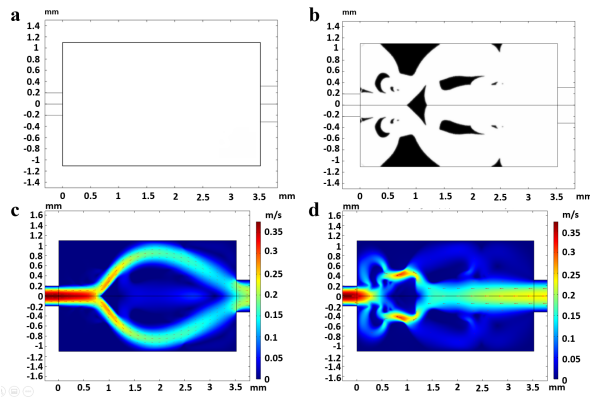


Fig. 2. (a) Computational domain for topology optimization; (b) fluidic diode geometry after topology optimization; (c) velocity contours of forward flow through the fluidic diode; (d) velocity contours of backward flow through the fluidic diode.

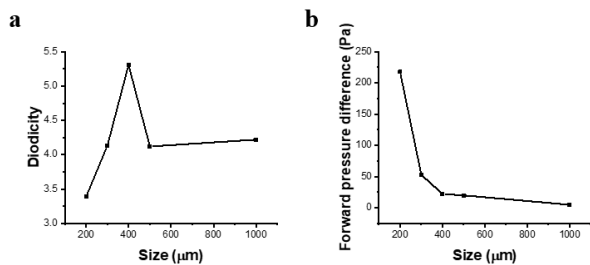


Fig. 3. (a) Highest diodicity of Tesla-type fluidic diode of different sizes; (b) pressure difference of fluidic diode with highest diodicity of different sizes.

The resulting geometry with the highest diodicity is shown in Fig. 2b. This figure also shows the geometry of a typical Tesla-type diode. The through-flow velocity contours for forward and backward flows through the fluidic diode are shown in Figures 2c and 2d. The backward flow is divided into several tributaries which then interact with one another at their confluence, leading to more resistance in the backward flow than in the forward flow. The diodicity of the fluidic diode is calculated by the ratio of backward flow pressure drop to forward flow pressure drop. It is 5.31 in this work.

Fig. 3a shows the optimized diodicity of fluidic diodes of different inlet sizes. The highest diodicity appears with an inlet size of $400\ \mu\text{m}$. The diodicity of smaller fluidic diodes is limited by the feature sizes, which has a great effect on the device fabrication while the diodicity of larger fluidic diodes is limited by the degrees of freedom during the optimization calculation. Too many elements leads to excessive degrees of freedoms and failure of convergence. Fig. 3b shows the corresponding forward pressure difference of fluidic diodes of different channel inlet sizes. The smaller pressure difference means smaller flow resistance and lower power needed to drive the pump. As the size of fluidic diode increases, the pressure difference first decreases, then tends to level off. The fluidic diode with an inlet chamber size of $400\ \mu\text{m}$ was selected for further simulation.

Topology optimization was performed on a two-dimensional (infinite depth) geometry, which allows viscous forces on the side walls to be neglected. However, the height of the actual microchannel is limited and is always comparable to the other two dimensions. Thus, it is important to consider the effect

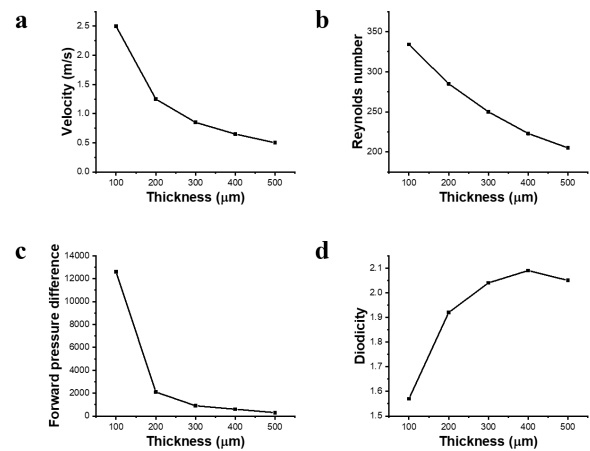


Fig. 4. The effects of thickness on (a) velocity, (b) Reynolds number, (c) pressure difference, and (d) diodicity of the Tesla-type designed fluidic diode.

of thickness on the performance of the designed fluidic diode. To address this, a three-dimensional analysis was performed by CFD simulation. When converting the simulation of the fluidic diode from two-dimensions to three, the mass flow rate of $0.1\ \text{g/s}$ was used for calculation and depths ranging from $100\ \mu\text{m}$ to $500\ \mu\text{m}$ were studied. Fig. 4 shows the velocity, Reynolds number, pressure difference, and diodicity of fluidic diodes of various thicknesses. The results show that larger thickness leads to smaller velocities and Reynolds numbers due to the fixed mass flow rate. The diodicity is reduced because of the smaller associated inertial forces. On the other hand, the effects of viscous forces are more significant when the thickness is less, leading to higher pressure differences but lower diodicities. The simulation was conducted for a valveless micropump using a $200\ \mu\text{m}$ thick microchannel.

Before the simulation of the Tesla-type valveless micropump with the chosen fluidic diode, the structure of the fluidic diode was simplified for lower complexity and easier fabrication. Fig. 5a shows the structure and diodicity of the original design. As shown in Fig. 5b, all structures smaller than $20\ \mu\text{m}$ were removed to avoid fabrication of high-aspect-ratio features, and the diodicity was reduced from 1.92 to 1.90. Small structures with little effect on diodicity were also removed, resulting in a diodicity of 1.89 (Fig. 5c). Any further simplification (as in Fig. 5d) leads to significant reduction of diodicity. Therefore, the structure in Fig. 5c was employed in the valveless micropump with Tesla-type fluid diodes.

Simulation of valveless micropumps was conducted by CFD. The geometry used for simulation is shown in Fig. 6a. The two fluidic diodes are connected by an actuator chamber attached to a PZT actuator and the other ends are connected to the inlet and outlet chambers. The thickness of fluidic diode and actuator chamber was set as $200\ \mu\text{m}$. The fluid parameters were set according to water at room temperature. The transient laminar flow model with the SIMPLE pressure treatment algorithm and second-order upwind interpolation was used for the simulation.

The diameter of the chamber having the attached PZT actuator was $10\ \text{mm}$. The amplitude of oscillation of the center of the actuator was set as $5\ \mu\text{m}$, matching optimum experimental results. The changes in displacement over time follows a

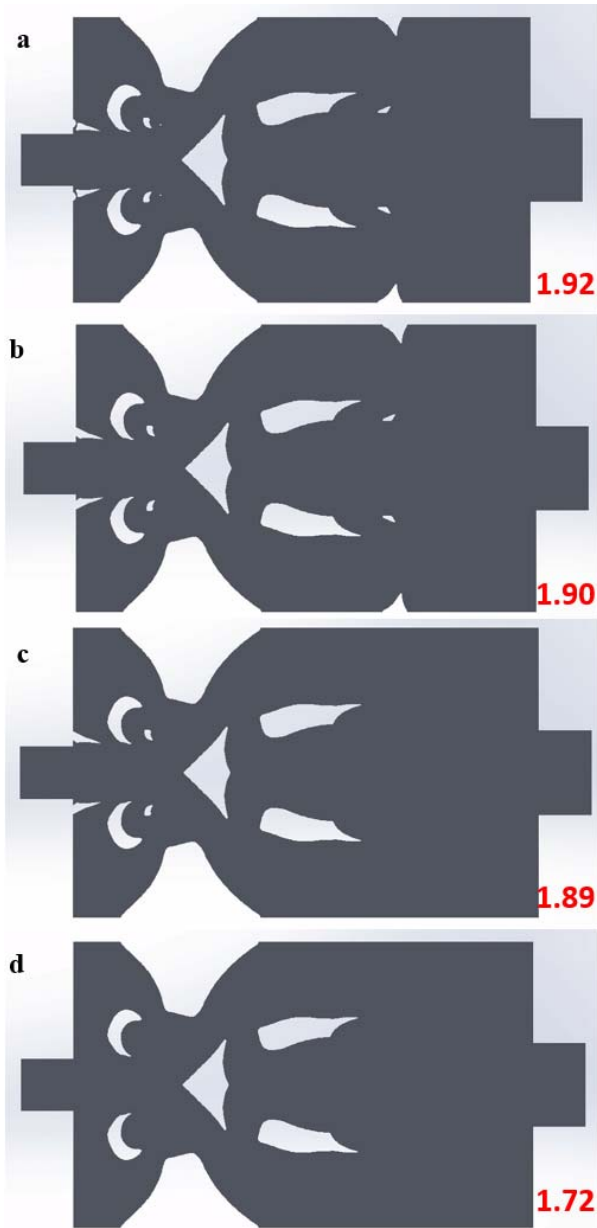


Fig. 5. Structure and diodicity of (a) original designed Tesla-type fluidic diode; (b) fluidic diode with small structure removed; (c) fluidic diode with unnecessary structure removed; (d) fluidic diode with critical structure removed.

sinusoidal wave function. The deflection profile of the PZT actuator can be divided into two sections: the inner section, with piezoelectric ceramics, and the outer section, with brass (see Fig. 6a). When a sinusoidal excitation voltage is applied to the PZT disc, the piezoelectric ceramic section vibrates. The brass section also vibrates. The deflection of these two sections can be described by the following equations [21]:

$$d_1(r) = d_{max} [1 + (b^2 r^2 - a^2 r^2) / (2a^2 b^2 \ln(a/b))] \sin(2\pi f t), \quad (0 \leq r \leq a) \quad (1)$$

$$d_2(r) = d_{max} [(b^2 + 2b^2 \ln(r/b) - r^2) / (2b^2 \ln(a/b))] \sin(2\pi f t), \quad (a \leq r \leq b) \quad (2)$$

where the d_1 and d_2 are the deflections of the inner and outer sections, respectively; d_{max} is the amplitude of the membrane center, which is set as $5 \mu\text{m}$; a is the radius of the inner

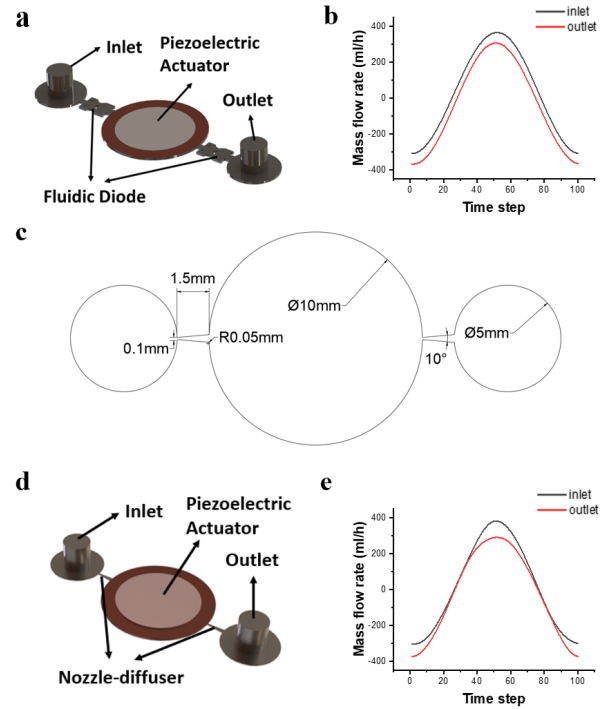


Fig. 6. (a) a schematic of the Tesla-type valveless micropump; (b) a plot of the mass flow rate for the Tesla-type valveless micropump; (c) critical parameters for the nozzle-diffuser type valveless micropump; (d) a schematic of the nozzle-diffuser type valveless micropump; (e) a plot of the mass flow rate for the nozzle-diffuser valveless micropump.

section, which is 3.75 mm ; b is the diameter of outer section, which is 5 mm ; f is the excitation frequency, which is 200 Hz .

Dynamic meshing with a User Defined Function (UDF) was applied to describe the movement of the piezoelectric actuator. The pressures of the inlet and outlet surfaces were set to zero and the mass flow rates at the inlet and outlet surfaces were monitored. A mesh sensitivity study was performed first to make sure that the results were independent of mesh quantity, and a mesh with 4.2 million nodes was chosen for the simulations. Each cycle was divided into 100 time-steps, leading to a time step size of $50 \mu\text{s}$. The details for the mesh and time-step independence studies can be found in the supplemental materials.

The mass flow rate through the micropump with the fluidic diodes in the inlet and outlet passages was calculated, as shown in Fig. 6b. The positive mass flow means water flow into the micropump, while the negative mass flow means the water flow out of the micropump. It can be found from the figure that when the water is pumping out, the outlet has a higher mass flow rate, and the inlet has a higher mass flow rate when the water is pumping in. The mass flow rate difference between inlet and outlet, integrated over time, leads to the net mass flow rate of the micropump. The net mass flow rate of 31.3 ml/h was calculated as the cycle average.

The same simulation was performed on the nozzle-diffuser type valveless micropump. The critical parameters of the nozzle-diffuser are shown in Fig. 6c, obtained from work done by He *et al.* [22]. The other parameters are the same as those of the Tesla-type fluidic diode-based valveless micropump. Fig. 6d shows the structure of the micropumps used for the simulation.

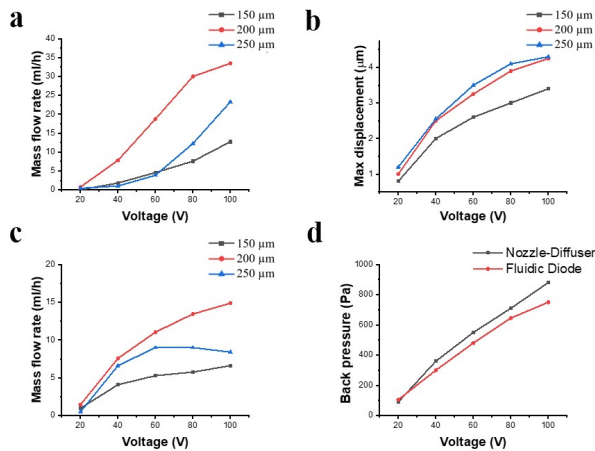


Fig. 7. (a) Mass flow rate of the fluidic diode-based valveless micropump in various thicknesses; (b) the maximum displacement of the center of the PZT actuator for the fluidic diode-based valveless micropump in various thickness; (c) the mass flow rate of the nozzle-diffuser type valveless micropump in various thicknesses; (d) back pressure of the two different types of valveless micropumps 200 μm thick.

The mass flow rate of the nozzle-diffuser type valveless micropump was calculated based on the inlet and outlet mass flow rate difference, as shown in Fig. 6e. The simulated mass flow rate was 20.6 ml/h, 34.2% lower than with the Tesla-type fluidic diode-based valveless micropump. Comparing Figures 6b and 6e shows that both micropumps have high diodicity at high flow velocity while the Tesla-type fluidic diode-based valveless micropump has better performance at lower flow rates. This is consistent with the high diodicity of the designed Tesla-type fluidic diode under low Reynolds number conditions.

To verify the simulation results and optimize the working conditions of the valveless micropumps, both the Tesla-type fluidic diode and the nozzle-diffuser type valveless micropumps of various thicknesses were fabricated using the process described in Fig. 1a.

Fig. 7a shows the measured mass flow rates of the Tesla-type diode micropump operating under different excitation voltages. As discussed previously, there is no inlet-to-outlet pressure difference for this flow measurement. As shown, the mass flow rate increases as the excitation voltage increases. The reason can be found in Fig. 7b, showing the maximum displacement of the center of the PZT actuator under different excitation voltages. Higher excitation voltage leads to larger displacements of the PZT actuator, resulting in increased mass flow rates. This micropump of 200 μm thickness has a higher mass flow rate than the ones of 150 μm and 250 μm thicknesses. This suggests that the inertial and viscous forces reach a balance under an optimum thickness of 200 μm , producing higher diodicity and mass flow rate. The different flow rates when the inlet-to-outlet pressure difference is zero, different maximum displacement of the PZT actuator, and different pressure differences when flow rate is zero are shown in Figures 7a, 7b, and 7c, respectively, each for three different thicknesses. The highest mass flow rate achieved is 33.5 ml/h. The difference between simulation results and experimental data is about 7%, lending credibility to the results from CFD simulation.

Three nozzle-diffuser type valveless micropumps with different thicknesses were fabricated for comparison. The mass

flow rates of the nozzle-diffuser type valveless micropumps in different thickness were also measured, as shown in Fig. 7c. As with the Tesla-type fluidic diode-based micropumps, the mass flow rate increases with excitation voltage and the micropump of 200 μm thickness has a higher mass flow rate, compared to the pumps of other thicknesses. The highest mass flow rate achieved by the nozzle-diffuser type valveless micropumps is 14.9 ml/h, 44% of the valveless micropump with the Tesla-type designed fluidic diodes. Comparing the experimental results with the simulation results shown in Fig 6e, the computational calculation is 38% overestimated. The gap between measurements and computation is mainly due to the lower displacement of the actuator in real testing. The vibration amplitude of the actuator for the nozzle-diffuser and designed fluidic diode valveless pump was set the same in CFD simulation. However, the nozzle-diffuser has a higher forward pressure difference than the designed fluidic diode, therefore the PZT actuator cannot achieve the same amplitude as diode-based micropumps do when the same voltage is applied.

The pressure differences of the two different types of valveless micropumps, both 200 μm thick, were measured and compared. Recall that this measurement was taken without flow. As shown in Fig. 7d, the nozzle-diffuser type micropump has a higher pressure difference than the Tesla-type fluidic diode-based micropump. This is as expected because the designed Tesla-type fluidic diode has a small pressure difference, as shown in Fig. 4c. Although the designed Tesla-type fluidic diode has high diodicity, its pressure differences are relatively low. However, the mismatch of pressure difference between the two valveless micropumps is only around 10%. Relative to the 2.2 times enhancement of the mass flow rate for the Tesla-type diode micropump, this small difference of pressure drop is justified.

IV. CONCLUSION

This work provides an efficient design process for developing a high-performance fluidic diode-based valveless micropump. A two-dimensional fluidic diode was first obtained by topology optimization. The diodicity reached 5.31 with a Reynolds number of 100. Then the thickness and layout of the Tesla-type designed fluidic diode were optimized and deployed in the valveless micropump. The performance of the proposed valveless micropump was evaluated by both CFD simulation and experiments. The result shows that the high diodicity of the Tesla-type designed fluidic diode leads to better performance at low Reynolds numbers among the two valveless micropumps. It was proven that the valveless micropump of 200 μm thickness with the designed Tesla-type fluidic diode can achieve 2.2 times the mass flow rate of the traditional nozzle-diffuser type valveless micropump. A large number of applications will benefit from the high flow rate of the designed valveless micropump. For example, more efficient mixing caused by stronger convection can be expected when the valveless micropump is used for mixing of microfluidic streams. Also, higher throughput for drug delivery and stronger actuation for ‘organs on a chip’ can be expected.

ACKNOWLEDGMENT

The numerical part of this work was carried out using computing resources at the University of Minnesota Supercomputing Institute.

REFERENCES

- [1] S. Hanasoge, P. J. Hesketh, and A. Alexeev, "Microfluidic pumping using artificial magnetic cilia," *Microsyst. Nanoeng.*, vol. 4, no. 1, pp. 1–9, Dec. 2018.
- [2] R. R. Gidde, P. M. Pawar, and V. P. Dhamgaye, "Fully coupled modeling and design of a piezoelectric actuation based valveless micropump for drug delivery application," *Microsyst. Technol.*, vol. 26, no. 2, pp. 633–645, Feb. 2020.
- [3] S. Mi, H. Pu, S. Xia, and W. Sun, "A minimized valveless electro-magnetic micropump for microfluidic actuation on organ chips," *Sens. Actuators A, Phys.*, vol. 301, Jan. 2020, Art. no. 111704.
- [4] E. Stemme and G. Stemme, "A valveless diffuser/nozzle-based fluid pump," *Sens. Actuators A, Phys.*, vol. 39, no. 2, pp. 159–167, Nov. 1993.
- [5] K. Mohammadzadeh, E. M. Kolahdouz, E. Shirani, and M. B. Shafii, "Numerical study on the performance of Tesla type microvalve in a valveless micropump in the range of low frequencies," *J. Micro-Bio Robot.*, vol. 8, nos. 3–4, pp. 145–159, Dec. 2013.
- [6] X. N. Jiang, Z. Y. Zhou, X. Y. Huang, Y. Li, Y. Yang, and C. Y. Liu, "Micronozzle/diffuser flow and its application in micro valveless pumps," *Sens. Actuators A, Phys.*, vol. 70, nos. 1–2, pp. 81–87, Oct. 1998.
- [7] H. A. Dereshgi and M. Z. Yildiz, "Investigation of electro-mechanical factors effecting piezoelectric actuator for valveless micropump characteristics," *J. Eng. Sci. Technol.*, vol. 13, no. 9, pp. 2843–2856, 2018.
- [8] A. Chandrasekaran and M. Packirisamy, "Geometrical tuning of micro-diffuser/nozzle for valveless micropumps," *J. Micromech. Microeng.*, vol. 21, no. 4, Apr. 2011, Art. no. 045035.
- [9] K.-S. Yang, T.-F. Chao, I. Y. Chen, C.-C. Wang, and J.-C. Shyu, "A comparative study of nozzle/diffuser micropumps with novel valves," *Molecules*, vol. 17, no. 2, pp. 2178–2187, Feb. 2012.
- [10] F. K. Forster, R. L. Bardell, A. P. Blanchard, M. A. Fromowitz, and N. R. Sharma, "Micropumps with fixed valves," U.S. Patent 5876 187, Mar. 2, 1999.
- [11] S. Derakhshan *et al.*, "Performance improvement and two-phase flow study of a piezoelectric micropump with Tesla nozzle-diffuser microvalves," *J. Appl. Fluid Mech.*, vol. 12, no. 2, pp. 341–350, Mar. 2019.
- [12] E. M. Kolahdouz, "Design and fabrication of a piezoelectrically actuated micropump using modified Tesla type microvalves," M.S. thesis, Dept. Mech. Eng., Isfahan Univ. Technol., Isfahan, Iran, 2010.
- [13] Q. Yan, Y. Yin, W. Sun, and J. Fu, "Advances in valveless piezoelectric pumps," *Appl. Sci.*, vol. 11, no. 15, p. 7061, Jul. 2021.
- [14] O. Sigmund and K. Maute, "Topology optimization approaches," *Struct. Multidisciplinary Optim.*, vol. 48, no. 6, pp. 1031–1055, Dec. 2013.
- [15] J. Alexandersen and C. S. Andreasen, "A review of topology optimisation for fluid-based problems," *Fluids*, vol. 5, no. 1, p. 29, Mar. 2020.
- [16] S. Lin, L. Zhao, J. K. Guest, T. P. Weihs, and Z. Liu, "Topology optimization of fixed-geometry fluid diodes," *J. Mech. Design*, vol. 137, no. 8, Aug. 2015, Art. no. 081402.
- [17] Y. Sato, K. Yaji, K. Izui, T. Yamada, and S. Nishiwaki, "Topology optimization of a no-moving-part valve incorporating Pareto frontier exploration," *Struct. Multidisciplinary Optim.*, vol. 56, no. 4, pp. 839–851, Oct. 2017.
- [18] Y. Deng, Z. Liu, P. Zhang, Y. Wu, and J. G. Korvink, "Optimization of no-moving part fluidic resistance microvalves with low Reynolds number," presented at the IEEE 23rd Int. Conf. Micro Electro Mech. Syst. (MEMS), Hong Kong, Jan. 2010.
- [19] M. P. Bendsoe and O. Sigmund, *Topology Optimization: Theory, Methods, and Applications*. Berlin, Germany: Springer, 2013.
- [20] T. H. Yoon, S. H. Park, K. I. Min, X. Zhang, S. J. Haswell, and D.-P. Kim, "Novel inorganic polymer derived microreactors for organic microchemistry applications," *Lab a Chip*, vol. 8, no. 9, pp. 1454–1459, 2008.
- [21] S. Yang, S. Q. Yuan, S. C. Cai, D. D. Wei, and X. H. He, "A valveless piezoelectric micropump based on Coanda effect," *Trans. Chin. Soc. Agricult. Eng.*, vol. 45, pp. 343–348, Mar. 2014.
- [22] X. He, J. Zhu, X. Zhang, L. Xu, and S. Yang, "The analysis of internal transient flow and the performance of valveless piezoelectric micropumps with planar diffuser/nozzles elements," *Microsyst. Technol.*, vol. 23, no. 1, pp. 23–37, Jan. 2017.
- [23] P. Zhou, T. Zhang, T. Simon, and T. Cui, "A fluidic diode and its application to a valveless micropump," presented at the IEEE 34th Int. Conf. Micro Electro Mech. Syst. (MEMS), Jan. 2021.



Peng Zhou was born in Ningguo, Anhui, China, in 1993. He received the B.S. degree from the Department of Mechanical Engineering, Beijing Institute of Technology, China, in 2015, and the M.S. degree in mechanical engineering from Purdue University Northwest, USA. He is currently pursuing the Ph.D. degree with the Department of Mechanical Engineering, University of Minnesota, guided by Prof. T. Cui.

His research interests include the photocatalytic water purification and MEMS-based microsensors for both environmental and biomedical applications.



Tianyi Zhang was born in Qinhuangdao, Hebei, China, in 1990. He received the B.S. and Ph.D. degrees from the Department of Mechanical Engineering, Xi'an Jiaotong University, Xi'an, Shanxi, China, in 2013 and 2019, respectively.

He spent one year as a Visiting Scholar at the University of Minnesota, where he is currently a Post-Doctoral Associate with the Department of Mechanical Engineering. His research interests include vibration mode coupling in micromechanical resonators and oscillators and mass transport in electrochemical sensing applications.



Terrence W. Simon received the B.S. degree in mechanical engineering from Washington State University, Pullman, WA, USA, in 1968, the M.S. degree in mechanical engineering from the University of California at Berkeley, Berkeley, CA, USA, in 1971, and the Ph.D. degree in mechanical engineering from Stanford University, Stanford, CA, USA, in 1980.

He is the Ernst G. Eckert Professor with the Department of Mechanical Engineering. His major research interests include experiments, computation, and visualization of heat, mass, and momentum transfer in laminar, turbulent, transitional, and unsteady flows, including flows through porous media and processes with phase change. Applications range from flow and heat transfer in plasma cutting tools and plasma flow actuators, electronics and optics, Stirling and gas turbine engines, and MW-level grid energy storage systems.

Dr. Simon is an Active Member of the American Society of Mechanical Engineers (including a past five-year term as the Senior Technical Editor of the *Journal of Heat Transfer*), the International Centre for Heat and Mass Transfer (in which he is now the President and has served on the Executive Committee), and the American Society of Thermal and Fluids Engineers (for which he co-chaired the International Workshop on Heat Transfer in 2017).



Tianhong Cui (Senior Member, IEEE) received the B.S. degree in mechanical engineering from the Nanjing University of Aeronautics and Astronautics in 1991 and the Ph.D. degree in mechanical engineering from the Chinese Academy of Sciences in 1995.

He is currently a Distinguished McKnight University Professor at the University of Minnesota. From 1995 to 2003, he held research or faculty positions at Tsinghua University, the University of Minnesota, the National Laboratory of Metrology, Japan, and Louisiana Tech University, before he joined the Faculty at the University of Minnesota. His research interests include MEMS and NEMS. He has more than 340 archived publications in scientific journals and prestigious conferences. He is an Adjunct Professor at Mayo Clinic, a Distinguished Visiting Fellow at the University of Cambridge, and a Distinguished Visiting Professor at the University of Paris-Est, France.

Dr. Cui is a fellow of the American Society of Mechanical Engineering (ASME). He is the Founding Executive Editor-in-Chief of *Microsystems & Nanoeengineering* (Nature). He is also serving as the Founding Editor-in-Chief of the first AAAS/Science Partner Journal titled *Research*.